Nonlocal Calculus-Based Macroscopic Traffic Model: Development, Analysis, and Validation

PUSHKIN KACHROO[1] (Senior Member, IEEE), SHAURYA AGARWAL[2] (Senior Member, IEEE), ANIMESH BISWAS[3], AND ARCHIE J. HUANG[2] (Member, IEEE)

[1]Department of Electrical and Computer Engineering, University of Nevada Las Vegas, Las Vegas, NV 89154, USA

[2]Civil, Environmental and Construction Engineering Department, University of Central Florida, Orlando, FL 32826, USA

[3]Department of Mathematics, University of Nebraska at Lincoln, Lincoln, NE 68588, USA

CORRESPONDING AUTHOR: S. AGARWAL (e-mail: shaurya.agarwal@ucf.edu)

ABSTRACT Nonlocal calculus-based macroscopic traffic models overcome the limitations of classical local models in accurately capturing traffic flow dynamics. These models incorporate "nonlocal" elements by considering the speed as a weighted mean of downstream traffic density, aligning it more closely with realistic driving behaviors. The primary contributions of this research are manifold. Firstly, we choose a nonlocal LWR model and Greenshields fundamental diagram and prove that this traffic flow model satisfies the well-posed conditions. Furthermore, we prove that the chosen model maintains bounded states, laying the groundwork for developing numerically stable schemes. Subsequently, the efficacy of the proposed nonlocal model is evaluated through extensive field validation using real traffic data from the NGSIM dataset and developing a stable numerical scheme. These validation results highlight the superiority of the nonlocal model in capturing traffic characteristics compared to its local counterpart and establish its enhanced accuracy in reproducing complex traffic behavior. Therefore, this research expands both the theoretical constructs within the field and substantiates its practical applicability.

INDEX TERMS Macroscopic traffic model, nonlocal calculus, nonlocal LWR model.

I. INTRODUCTION

CLASSIC macroscopic models such as the LWR model $\partial_t \rho(t, x) + \partial_x f(\rho(t, x)) = 0$, where $\rho : R^+ \times [a, b] \to [0, \rho_m]$ is the time and space varying traffic density defined on a road segment $[a, b]$ and where the values of the function output reside in $[0, \rho_m]$, ρ_m being the jam density. The density-dependent traffic flow is $f(\rho)$ and is given as the product of density-dependent speed $v(\rho)$ and density as $f(\rho) = \rho v(\rho)$.

The problem with this model is in the velocity term $v(\rho(t, x))$ as the velocity at (t, x) is the function of traffic density ρ at (t, x). This means that there is no *look-ahead behavior* of the driver in the model. There are two ways to deal with it. One way is to add a gradient term to the velocity function as $v(\rho, \partial_x \rho) = v_0(\rho) + k \partial_x \rho$. This converts the original hyperbolic LWR PDE into a diffusive (parabolic) one. However, the problem is that the model is still local,

and the velocity still depends on completely local traffic behavior at the same (t, x).

The other method that can be used employs a nonlocal velocity effect. An example is the model studied in [1], and [2]. The model is $\partial_t \rho(t, x) + \partial_x[\rho(t, x)v(\rho(t, x) *_d w_d(x))] = 0$, where $*_d$ is the *downstream* convolution defined as $\rho(t, x) *_d w_d(x) = \int_x^{x+d} \rho(t, y)w_d(y - x)dy$. Here $w_d(x)$ is a nondecreasing probability function, i.e., $\int_{\mathbb{R}} w_d(x)dx = 1$, with support on $[0, d]$. This model clearly takes into account the lookahead nonlocal nature of driving.

There is a great deal of recent development in the topic of extending traffic models and conservation laws to nonlocal versions [3], [4], [5], [6], [7], [8], [9], [10], [11]. This makes sense as the actual reality and the physics of the phenomenon clearly indicate the driver's view of integrating traffic conditions in front, which corresponds to the spatial integration of local traffic density in front of the driver.

Research Gaps: The development of a nonlocal LWR model and its usage for practical applications requires

The review of this article was arranged by Associate Editor Yajie Zou.

addressing some issues. Firstly, the well-posedness is an essential property of a partial differential equation model. It entails a theorem of the existence, uniqueness of its solution, and the continuity of the solution to its initial condition. The chosen model must be well-posed for it to be useful. Secondly, a prevailing *limitation* in numerous numerical schemes for nonlocal models is the inability to ensure that the original bounds imposed on the traffic flow are preserved throughout its evolution [11]. This constraint is critical for practical applications, particularly the upper bound on traffic jam density, which originates from the physical principles governing traffic modeling. Lastly, field validations are required to compare the efficacy of local and nonlocal models in capturing the complex traffic phenomenon.

Contributions: This paper addresses the research gaps mentioned earlier. Specifically, it contributes to the field of traffic flow modeling as follows.

1) We demonstrate the well-posedness of the adopted nonlocal LWR model and the Greenshields fundamental diagram by proving (Theorems 2 and 3) that they satisfy the well-posedness conditions provided in [1], and [2].

2) We resolve the boundedness issue through Lemma 1. By proving the Lemma, we demonstrate that the nonlocal LWR model adheres to the boundedness without violation, enabling the construction of stable numerical schemes.

3) We implement an adapted Lax-Friedrichs algorithm to generate numerically stable, approximate solutions. The schemes were designed using two look-ahead kernels.

4) Finally, the practical effectiveness and robustness of our proposed nonlocal model are substantiated through a thorough field validation using real-world traffic data from the NGSIM dataset. With additional analysis of the convolution window size and model performance comparison, we showcase the developed models' superior performance and utility in reconstructing the field data.

II. BACKGROUND

In this section, we will illustrate a nonlocal version of the traffic model originally developed by Lighthill, Whitham, and Richards called the LWR model [12], [13], [14]. The speed relationship with density can be linear (Greenshield's model, [15]), logarithmic model (Greenberg model, [16]), exponential (Underwood model, [17]), bell-shaped (Drake model, [18]), etc. The models can also exhibit multiple phases [5], [19] and use statistical Physics [20]. There also exist higher-order traffic flow dynamics and traffic network models [21].

A. NONLOCAL LWR MODEL

The nonlocal model that we will use is illustrated in Figure 1. Traffic density $\rho(t, x)$ is a time-varying scalar field defined
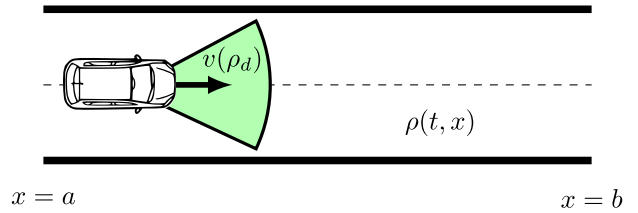

FIGURE 1. Nonlocal Traffic Density Field.

on $x \in [0, \ell]$, where $\rho(t, x) \in [0, \rho_m]$, ρ_m being the jam density, i.e., the traffic density when the traffic speed is zero.

The variable $\rho_d(t, x)$ is the smoothed look-ahead traffic density obtained by a convolution of $\rho(t, x)$ with a look-ahead kernel function $\eta(x)$. The kernel function $\eta(x)$ generalizes the probability density function $w_d(x)$, defined earlier.

$$\rho_d(t, x) = \rho(t, x) \circledast \eta(x) = \int_{x}^{x+d} \rho(t, y)\eta(y - x)dy \quad (1)$$

where symbol $\circledast$ has been used for a look-ahead convolution. The kernel $\eta(x) \in \mathbf{C}^n([0, d]; \mathbb{R}^+)$ is a non-increasing function and has the following property.

$$\int_{0}^{d} \eta(x)dx = 1 \quad (2)$$

The conservation law is

$$\partial_t \rho(t, x) + \partial_x[\rho(t, x)v(\rho_d)] = 0 \quad (3)$$

As mentioned previously, we can use one of the models for $v(\rho_d)$ as a function of ρ_d. Without loss of generality, we will use Greenshields relationship in this paper:

$$v(\rho_d) = v_f \left(1 - \frac{\rho_d}{\rho_m}\right) \quad (4)$$

where v_f is the free low speed, and ρ_m is the jam density.

B. A GENERAL INITIAL BOUNDARY VALUE PROBLEM

In this section, we define the sense in which the solution of the conservation law with its initial condition and boundary conditions has to be considered for it to be well-posed [22]. However, the model used in [22] is generic, and we will adapt it specifically for developing a nonlocal initial boundary value problem for LWR paired with Greenshields fundamental diagram.

In order for the model that we present to be useful for applications, the model must be well-posed; otherwise, the model becomes useless for any meaningful analysis. Well-posedness is an important property of a partial differential equation (PDE). A well-posed PDE entails a theorem of the existence and uniqueness of its solution as well as the continuity of the solution to its initial condition. Specifically, the model must have at least one solution for the given initial condition, which refers to the existence of the solution. Moreover, there should only be one solution for the given initial condition. The solution should be stable

to initial conditions, which means that small changes to initial conditions should produce only small changes to the evolution of the system trajectories. To this end, Definition 1 is a weak entropy (Kruzhkov) solution. Definition 1 and Theorem 1 illustrate the requirements for the model to be well-posed.

1) MODEL DESCRIPTION

The general initial boundary value problem is

$$\partial_t\rho(t,x) + \partial_x f(t,x,\rho,\rho(t,x)*\eta(x)) = 0, \quad (t,x) \in \mathbb{R}^+ \times (a,b)$$
$$\rho(0,x) = \rho_0, \quad x \in (a,b)$$
$$\rho(t,a) = \rho_a(t), \quad t \in \mathbb{R}^+$$
$$\rho(t,b) = \rho_b(t), \quad t \in \mathbb{R}^+ \qquad (5)$$

$f \in \mathbf{C}^2(\mathbb{R}^+ \times [a,b] \times \mathbb{R} \times \mathbb{R}; \mathbb{R})$ satisfies

$$f(t,x,0,r) = 0, \quad \forall t,x,r,$$
$$\sup_{t,x,\rho,r} |\partial_\rho f(t,x,\rho,r)| < K_1,$$
$$\sup_{t,x,r} |\partial_x f(t,x,\rho,r)| < K_2|\rho|,$$
$$\sup_{t,x,r} |\partial_r f(t,x,\rho,r)| < K_2|\rho|,$$
$$\sup_{t,x,r} |\partial_{xx} f(t,x,\rho,r)| < K_2|\rho|,$$
$$\sup_{t,x,r} |\partial_{xr} f(t,x,\rho,r)| < K_2|\rho|,$$
$$\sup_{t,x,r} |\partial_{rr} f(t,x,\rho,r)| < K_2|\rho| \qquad (6)$$

We have $K_1 > 0$, $K_2 > 0$ which are constants, and $\eta \in (\mathbf{C}^1 \cap \mathbf{W}^{1,\infty})(\mathbb{R};\mathbb{R})$ with

$$\int_{\mathbb{R}} \eta(x)dx = 1 \qquad (7)$$

Conservation laws generally have discontinuities due to shock waves and contact discontinuities, as well as rarefaction waves, which require the notion of weak and vanishing viscosity or entropy solutions. The initial and boundary values also need to be understood in the weak sense [22], [23], [24] as shown below. For the sake of completeness, we borrow the following definition for this notion of the solution from [22].

Definition 1: Given the initial condition $\rho_0 \in \mathbf{L}^\infty((a,b);\mathbb{R})$, and the two boundary conditions $\rho_a, \rho_b \in \mathbf{L}^\infty(\mathbb{R}^+;\mathbb{R})$, $\rho \in BV(\mathbb{R}^+ \times (a,b);\mathbb{R})$ is a weak entropy solution in the sense of Kruzhkov, if $\forall \phi \in \mathbf{C}_0^1(\mathbb{R}^2;\mathbb{R}^+)$, and $\forall \kappa \in \mathbb{R}$, we have

$$\int_0^\infty \int_a^b \left(|\rho - \kappa|\partial_t\phi + \mathrm{sgn}(\rho - \kappa)\big[f(t,x,\rho,r(t,x)) \right.$$
$$\left. - f(t,x,\kappa,r(t,x))\big]\partial_x\phi \right.$$
$$\left. - \mathrm{sgn}(\rho - \kappa)\frac{d}{dx}f(t,x,\kappa,r(t,x))\phi \right)dxdt$$
$$+ \int_a^b |\rho_0 - \kappa|\phi(0,x)dx$$
$$+ \int_0^\infty \mathrm{sgn}(\rho_a - \kappa)\big[f(t,x,\rho(t,a+),r(t,a))$$
$$- f(t,x,\kappa,r(t,a))\big]\phi(t,a)dt$$

$$+ \int_0^\infty \mathrm{sgn}(\rho_b - \kappa)\big[f(t,x,\kappa,r(t,b))$$
$$- f(t,x,\rho(t,b-),r(t,b))\big]\phi(t,b)dt \geq 0 \qquad (8)$$

The initial and boundary conditions are understood in a weak sense consistent with entropy and satisfy trace property [23], [25], [26].

$$(\mathrm{sgn}(\rho(t,a+) - \kappa) - \mathrm{sgn}(\rho_a(t) - \kappa))$$
$$(f(t,a,\rho(t,a+),r(t,a)) - f(t,a,\kappa,r(t,a))) \leq 0,$$
$$\forall \kappa \in \mathbb{R}, x = a$$
$$(\mathrm{sgn}(\rho(t,b-) - \kappa) - \mathrm{sgn}(\rho_b(t) - \kappa))$$
$$(f(t,b,\rho(t,b-),r(t,b)) - f(t,b,\kappa,r(t,b))) \geq 0,$$
$$\forall \kappa \in \mathbb{R}, x = b \qquad (9)$$

2) WELL-POSEDNESS AND PROPERTIES

The well-posedness result and solution properties of the model given in Section II-B1. (titled, *Model*) are presented in the theorem below [22].

Theorem 1: Given the hypothesis and conditions of Equation (5), Equation (6), and Equation (7), $\rho_0 \in (\mathbf{L}^\infty \cap BV)((a,b);\mathbb{R}^+)$, $\rho_a, \rho_b \in (\mathbf{L}^\infty \cap BV)(\mathbb{R}^+;\mathbb{R}^+)$, then $\forall t > 0$, $\rho \in BV((0,t) \times (a,b);\mathbb{R}^+)$ is a weak entropy solution in the sense of Kruzhkov satisfying the conditions prescribed in Equation (8), and having the properties stated here. The properties provide bounds on the $\|\rho(t,\cdot)\|_{\mathbf{L}^\infty(a,b)}$, $\|\rho(t,\cdot)\|_{\mathbf{L}^1(a,b)}$, and $\|\rho(t,\cdot)\|_{TV(a,b)}$ norms.

$$\|\rho(t,\cdot)\|_{\mathbf{L}^\infty(a,b)} \leq e^{\mathcal{L}t}\|\rho_0\|_{\mathbf{L}^\infty(a,b)}$$
$$\|\rho(t,\cdot)\|_{\mathbf{L}^1(a,b)} \leq \|\rho_0\|_{\mathbf{L}^1(a,b)} + \alpha\big(\|\rho_a\|_{\mathbf{L}^1[0,t]} + \|\rho_b\|_{\mathbf{L}^1[0,t]}\big)$$
$$TV(\rho(t,\cdot);(a,b)) \leq e^{\kappa_1 t}TV(\rho_0;(a,b)) + \frac{\kappa_2}{\kappa_1}\big(e^{\kappa_1 t} - 1\big)$$
$$+ TV(\rho_a;[0,t]) + TV(\rho_b;[0,t]) \qquad (10)$$

Continuity of the solution in $\mathbf{L}^1(a,b)$ with respect to time is shown by

$$\|\rho(t_2,\cdot) - \rho(t_1,\cdot)\|_{\mathbf{L}^\infty(a,b)} \leq C(t_2)(t_2 - t_1) \qquad (11)$$

The uniqueness of the solution is obtained by the continuity property of the solution with respect to the initial and boundary data as shown in Equation (12) where ρ and σ are two solutions with initial data ρ_0 and σ_0, and the boundary data ρ_a, ρ_b, σ_a, and σ_b.

$$\|\rho(t,\cdot) - \sigma(t,\cdot)\|_{\mathbf{L}^1(a,b)}$$
$$\leq e^{\mathcal{S}t}\big[\|\rho_0 - \sigma_0\|_{\mathbf{L}^1(a,b)} + \kappa_4\big(\|\rho_a - \sigma_a\|_{\mathbf{L}^1[0,t]}$$
$$+ \|\rho_b - \sigma_b\|_{\mathbf{L}^1[0,t]}\big)\big] \qquad (12)$$

The terms α, $\mathcal{L}$, $\mathcal{S}$, κ_1, κ_2, κ_3, and κ_4 are all defined in [22].

III. ANALYSIS OF NONLOCAL INITIAL BOUNDARY VALUE LWR

In this section, we will apply the existing well-posedness results for the model shown in Section II-B2. to our chosen initial boundary value problem shown in Section II-A. In

other words, we prove that the chosen model - nonlocal LWR paired with Greenshields fundamental diagram - is well-posed.

$$\partial_t\rho(t,x) + \partial_x f(t,x,\rho,\rho(t,x) \circledast \eta(x)) = 0,$$
$$(t,x) \in \mathbb{R}^+ \times (a,b)$$
$$\rho(0,x) = \rho_0, \quad x \in (a,b),$$
$$\rho(t,a) = \rho_a(t), \quad \rho(t,b) = \rho_b(t), \quad t \in \mathbb{R}^+ \quad (13)$$

$f \in \mathbf{C}^2(\mathbb{R}^+ \times [a,b] \times \mathbb{R} \times \mathbb{R}; \mathbb{R})$ is given by

$$f(t,x,\rho,\rho(t,x) \circledast \eta(x))$$
$$= \rho v(\rho_d) = v_f \rho \left(1 - \frac{\rho_d}{\rho_m}\right)$$
$$= v_f \rho \left(1 - \frac{\int_x^{x+d} \rho(t,x)\eta(y-x)dy}{\rho_m}\right) \quad (14)$$

Now, we check the conditions on the flow f to be satisfied for our model.

A. FLOW CONDITIONS

The conditions to be satisfied and the corresponding analysis is presented next.

1) ZERO CONDITION

The condition to be satisfied is

$$f(t,x,0,r) = 0, \quad \forall t,x,r \quad (15)$$

which is clearly satisfied by substituting $\rho = 0$ into the formula for f provided in Equation (14).

2) FIRST ORDER CONDITIONS

The conditions to be satisfied are

$$\sup_{t,x,\rho,r} |\partial_\rho f(t,x,\rho,r)| < K_1,$$
$$\sup_{t,x,r} |\partial_x f(t,x,\rho,r)| < K_2|\rho|,$$
$$\sup_{t,x,r} |\partial_r f(t,x,\rho,r)| < K_2|\rho| \quad (16)$$

In order to prove $\sup_{t,x,\rho,r} |\partial_\rho f(t,x,\rho,r)| < K_1$, we first prove the following lemma.

Lemma 1: Given $\forall x \in (a,b), \ \rho_0(x) \in [0,\rho_m] \implies \forall t > 0, x \in (a,b), \ \rho(t,x) \in [0,\rho_m]$.

Proof: On any characteristic parameterized as $(t,x(t))$, we have

$$\partial_t\rho(t,x) + \partial_x f(t,x(t),\rho(t,x(t)),\rho_d(t,x(t))) = 0 \quad (17)$$

On the initial point of this characteristic, we obtain

$$|\rho_d(0,x(0))| = |[\rho(0,x) \circledast \eta(x)](x(0))|$$
$$= \left|\left[\int_x^{x+d}\rho(0,x)\eta(y-x)dy\right](x(0))\right|$$
$$\leq \rho_m \left|\left[\int_x^{x+d}\eta(y-x)dy\right](x(0))\right| = \rho_m \quad (18)$$

∎

Theorem 2: The solution to the nonlocal initial boundary value LWR presented in Equation (13) satisfies

$$\sup_{t,x,\rho,r} |\partial_\rho f(t,x,\rho,r)| < K_1 \quad (19)$$

Proof: We obtain the formula for $f(t,x,\rho,r)$ from Equation (14).

$$f(t,x,\rho,r) = \rho v(r) = v_f \rho \left(1 - \frac{r}{\rho_m}\right) \quad (20)$$

We have already shown in Lemma 1 that $r \in [0,\rho_m]$, and hence

$$f_\rho(t,x,\rho,r) = v(r) = v_f \left(1 - \frac{r}{\rho_m}\right) \leq v_f \quad (21)$$

∎

Theorem 3: The solution to the nonlocal initial boundary value LWR presented in Equation (13) satisfies

$$\sup_{t,x,r} |\partial_x f(t,x,\rho,r)| < K_2|\rho|,$$
$$\sup_{t,x,r} |\partial_r f(t,x,\rho,r)| < K_2|\rho| \quad (22)$$

Proof: We again use the formula for $f(t,x,\rho,r)$ from Equation (14). We easily see that $f_x(t,x,\rho,r) = 0$ and hence, the first condition is satisfied. For the second condition, we perform the following analysis:

$$|\partial_r f(t,x,\rho,r)| = \left|\partial_r\left[v_f\rho\left(1 - \frac{r}{\rho_m}\right)\right]\right| \leq \frac{v_f}{\rho_m}|\rho| \quad (23)$$

∎

3) SECOND ORDER CONDITIONS

The conditions to be satisfied are

$$\sup_{t,x,r} |\partial_{xx} f(t,x,\rho,r)| < K_2|\rho|,$$
$$\sup_{t,x,r} |\partial_{xr} f(t,x,\rho,r)| < K_2|\rho|,$$
$$\sup_{t,x,r} |\partial_{rr} f(t,x,\rho,r)| < K_2|\rho| \quad (24)$$

We see by using the formula for $f(t,x,\rho,r)$ from Equation (14) that all the three-second order partial derivatives are zero and, hence, trivially satisfy the second order conditions for the model.

B. NUMERICAL SCHEME AND KERNEL DESIGN

In [22], an adapted Lax-Friedrichs algorithm has been used to produce approximate solutions to the general model in order to prove the well-posedness by the application of Helly's compactness theorem. We divide our space interval (a,b) into n steps with the space increment Δx taken as $\Delta x = (b-a)/n$ and time increment Δt. Then based on (13), the time update difference equation is given by,

$$\rho[n+1,j] = \frac{1}{2}\left(\rho[n,j+1] + \rho[n,j-1]\right)$$
$$- \frac{\Delta t}{2\Delta x}\left[f(n,j+1,\rho_d[n,j+1])\right.$$
$$\left. - f(n,j-1,\rho[n,j-1])\right], \quad (25)$$

(a) The constant Kernel

(b) The linearly decreasing kernel
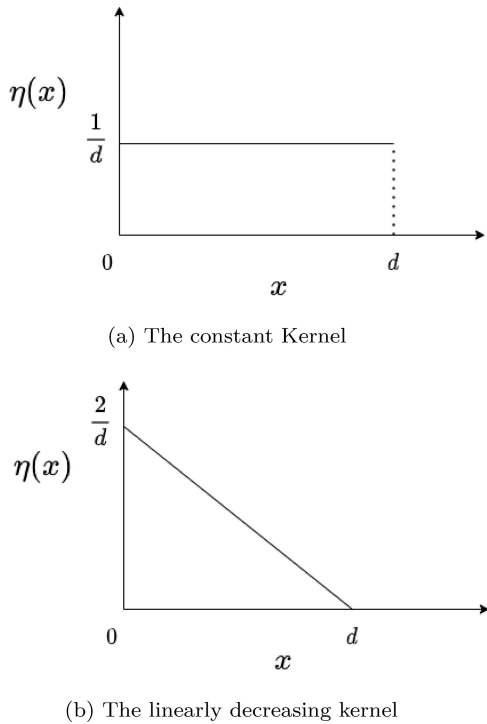
FIGURE 2. Convolution Kernels.

FIGURE 3. Spatio-temporal binning strategy.

where $\rho_d(t, x)$ is the nonlocal density at the point (t, x) as defined via look-ahead convolution. If $\eta(x)$ is the kernel defined on the interval $[0, d]$ where $d < (b - a)$, then to compute (1) numerically we use,

$$\rho_d[n, j] = \left(\sum_{i=0}^{n_d - 1} \rho[n, j + i]\eta[i] \right) \Delta x, \qquad (26)$$

where $n_d \Delta x = d$. Finally we use (14) to compute the flux. For our simulations, we use the following two types of the kernel.

1) The constant kernel, $\eta(x) = K\chi_{[0,d]}(x)$ such that $K = 1/d$. Here $\chi_{[0,d]}(x)$ is the characteristics function.
2) Linearly decreasing kernel, $\eta(x) = K(d-x)\chi_{[0,d]}$ such that $K = 2/d^2$.

In both cases, K is such that $\int_0^d \eta(x)dx = 1$. We notice that to compute ρ_d at the space variable j; we need to know the local density data ρ in the interval $[j, j + n_d - 1]$. Due to this reason, the right boundary conditions need to be 'thick.' We call this boundary condition to be nonlocal. Another important aspect of this numerical algorithm is stability. We observe that if we have Δt sufficiently small compared to Δx, then we almost always get a numerically stable solution due to the Courant-Friedrichs-Lewy condition [27]. While working with the real data, we implement a smaller time discretization than given in the dataset using a simple interpolation scheme. That scheme helps us to get numerically stable solutions for the nonlocal equation. The illustration of the convolution kernels is shown in Figure 2.
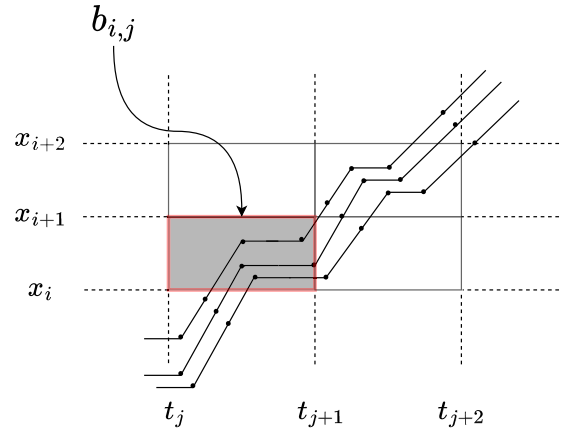
IV. FIELD VALIDATION
A. DATA DESCRIPTION
For this paper, we use traffic flow data of the US-101 freeway from the NGSIM dataset. The NGSIM program captured high-resolution vehicle trajectory video data at four locations between 2005 and 2006 [28]. In this program, freeway and urban arterial data were collected to assist the FHWA Traffic Analysis Tools Program. The two freeway segments are I-80 and US-101, whereas the two arterial segments are Lankershim Boulevard and Peachtree Street. A network of the synchronized digital camera was used to capture video data, which was translated into microscopic vehicle trajectory data via a customized software application called NGVIDEO. The temporal resolution of the NGSIM trajectory data is 100 ms. That translates to a sampling frequency of 10 Hz. These high-resolution vehicle trajectory data offer the exact location and detailed lane positions of each vehicle. In addition, it provides a vehicle's relative locations with respect to other vehicles in the study area.

Freeway Segments: Vehicle trajectories on a 1640ft long segment of $I-80$ in Emeryville, California, were captured from the seven synchronized digital video cameras on April 13, 2005. The 45 minutes long video data has three equal time segments from three different periods: 1) 4:00 p.m. to 4:15 p.m., 2) 5:00 p.m. to 5:15 p.m., and 3) 5:15 p.m. to 5:30 p.m. Vehicle trajectories on a 2100ft long segment of $US101$ (Hollywood Freeway) in Los Angeles, California, were captured from the eight cameras positioned on a 36-story building near to the freeway. The 45-minute video data has three equal time segments: 1) 7:50 a.m. to 8:05 a.m., 2) 8:05 a.m. to 8:20 a.m., and 3) 8:20 a.m. to 8:35 a.m. June 15, 2005. There is an on-ramp and an off-ramp at approximately 590ft (Ventura Boulevard) and 1280ft (Cahuenga Boulevard) locations, respectively, on the studied segment of $US101$. There is an on-ramp at approximately 400ft location on the studied segment of the $I-80$ highway. $US101$ has five main lanes and one auxiliary lane between the ramps in the studied areas, while $I-80$ has six mainlines, including a high occupancy lane.
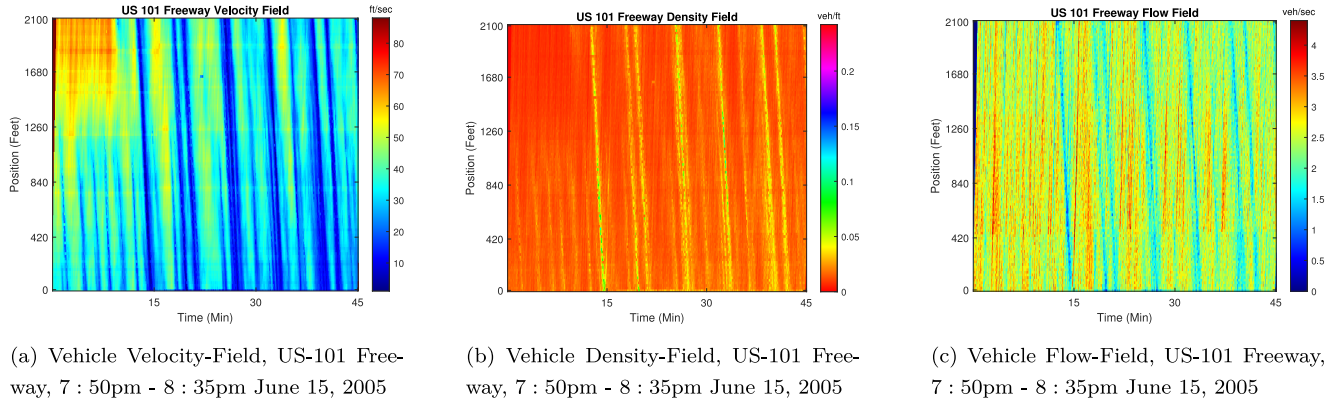
(a) Vehicle Velocity-Field, US-101 Free-
way, 7 : 50pm - 8 : 35pm June 15, 2005

(b) Vehicle Density-Field, US-101 Free-
way, 7 : 50pm - 8 : 35pm June 15, 2005

(c) Vehicle Flow-Field, US-101 Freeway,
7 : 50pm - 8 : 35pm June 15, 2005

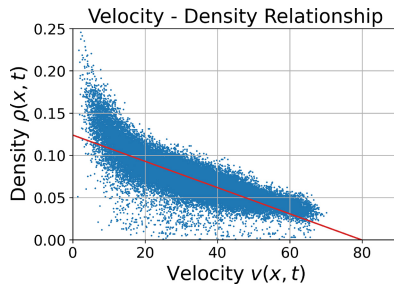**FIGURE 4.** The NGSIM Dataset, US-101 Freeway, 7:50pm - 8:35pm June 15, 2005.

FIGURE 5. Parameter Estimation of ρ_m and v_f.

Binning Strategy: NGSIM provides high-resolution vehicle trajectory data, which is in a Lagrangian setting. To construct velocity and density, the trajectories need to be converted into Eulerian bins. Some popular binning methods are provided in [29], [30]. Next, we briefly describe how to convert the vehicular traces to extract their spatio-temporal pattern. For example, let's define the 2D spatio-temporal domain or grids as $[0, l] \times [0, t]$ (see Figure 3). Any bin in the defined domain is characterized by

$$b_{i,j} = \left([i\Delta x, (i+1)\Delta x] \times [j\Delta t, (j+1)\Delta t] \right)_{i\in(1\cdots n_x), j\in(1\cdots n_t)} \tag{27}$$

where, the number of spatial bins $n_x = \frac{l}{\Delta x}$ and number of temporal bins $n_t = \frac{t}{\Delta t}$

$$\tilde{V}_{i,j} = Mean_{trace\in b_{i,j}}(V(trace)) \tag{28}$$

We assume that the traffic variables, such as velocity, density, or flow, are constant in each bin and that trajectories leave a trace on the spatio-temporal bins [29]. Considering $\Delta x = 20 ft/bin$ and $\Delta t = 5 sec/bin$, we have constructed velocity and density fields from NGSIM data of US-101 freeway, which is shown in Figure 4(a) and Figure 4(b). Figure 4(c) shows the corresponding flow field.

For estimating traffic parameters such as free-flow velocity and jam density, we utilized the density and velocity data set discussed earlier (see Figure 5). More details on the data can be found in [31], [32]. We first created a mapping between

the density and velocity data points and then applied linear regression. The y-intercept of the linear regression is the jam density, and the x-intercept is the free flow velocity. The estimated free-flow speed v_f is 80 feet per second, and the estimated jam density ρ_m is 0.12 vehicle per ft.

B. RESULTS AND DISCUSSION

We evaluate the effectiveness of the nonlocal LWR model paired with Greenshields fundamental diagram by performing the reconstruction of field data similar to our previous works using physics-informed deep learning (see [31], [33], [34]).

Now, we present the reconstructed density field by five models - one local LWR model and four nonlocal LWR models using the modified Lax-Friedrichs scheme described earlier. The nonlocal LWR models vary in configuration based on the kernel type (constant or linearly decreasing) and the width of the kernel window (60 ft and 200 ft).

The numerical solution setup of nonlocal LWR models using the modified Lax-Friedrichs scheme is shown in Figure 6. We use the initial condition (t = 0), the lower boundary condition (x = 0), and a thick upper boundary condition (for the computation of ρ_d) as the sole training input. For nonlocal models, the convolution kernel acts in the rolling look-ahead window shown in the figure.

We use the relative squared error (RSE) defined in (29) to measure the inaccuracy in the reconstructed density field. In (29), $\rho(x^{(j)}, t^{(j)})$ is the ground truth value of vehicle density at location $x^{(j)}$ and time $t^{(j)}$, and $\hat{\rho}(x^{(j)}, t^{(j)})$ is the estimated value of $\rho(x^{(j)}, t^{(j)})$ from the model output. N_1 is the total number of spatial locations, and N_2 is the total number of timestamps in the dataset:

$$RSE = \frac{\sum_{j=1}^{N_1 \cdot N_2} \left| \hat{\rho}(x^{(j)}, t^{(j)}) - \rho(x^{(j)}, t^{(j)}) \right|^2}{\sum_{j=1}^{N_1 \cdot N_2} \left| \rho(x^{(j)}, t^{(j)}) \right|^2} \times 100\% \tag{29}$$

The model with the smallest RSE is the nonlocal LWR model with a linearly decreasing kernel and a 60-ft look-ahead window. The evaluation of reconstruction results is
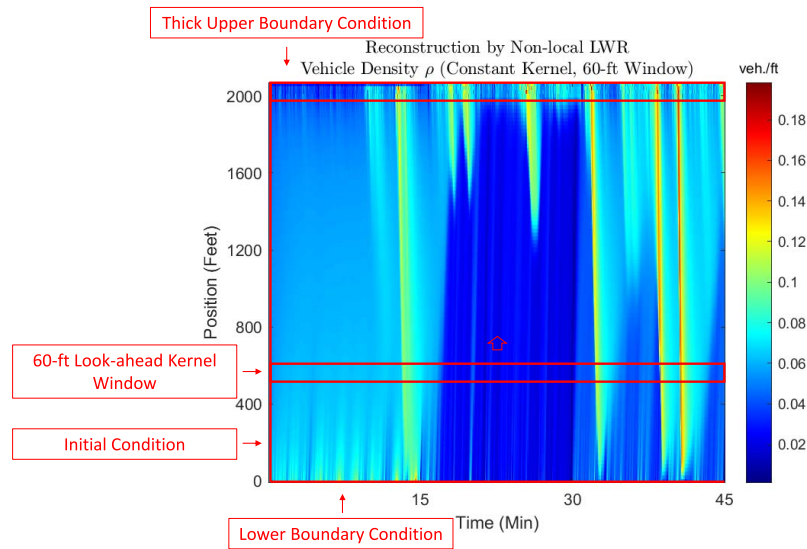
FIGURE 6. Reconstruction by nonlocal LWR with Look-ahead.

TABLE 1. Performance analysis: Inaccuracy in reconstruction.

	Model Type	Look-ahead Kernel	Convolution Window	RSE (%)
1	Local LWR	*N/A*	*N/A*	21.87
2	Nonlocal LWR	Constant	60-ft	21.32
3	Nonlocal LWR	Constant	100-ft	20.68
4	Nonlocal LWR	Linearly decreasing	60-ft	**13.71**
5	Nonlocal LWR	Linearly decreasing	100-ft	14.76

tabulated in Table 1, and the best performance is marked in *bold*.

For comparison, the original NGSIM data is plotted in Figure 7(a), and the reconstructed density fields are shown in the following figures: Figure 7(b) is the reconstruction by the local LWR model. Figure 7(c) and Figure 7(d) are generated by the nonlocal (constant kernel) LWR models with a look-ahead window of 60-ft and 100-ft, respectively. Similarly, Figure 7(e) and Figure 7(f) are individually produced by nonlocal (linearly decreasing kernel) LWR models with a look-ahead window of 60-ft and 100-ft.

Additionally, we perform the sensitivity analysis on the size of the convolution window and investigate its impact on the performance of the nonlocal models. The results are summarized in Table 2 and visualized in Figure 8.

From the sensitivity analysis result, we observe that the best-performing convolution window size for the linear kernel is 60 feet. The model with the linearly decreasing convolution kernel, which gradually discounts the weight of traffic information further away from the driver within the 60-ft convolution window, achieved the best RSE results among all models. If the convolution kernel is substituted with the constant version, then equal weights are assigned to the traffic state values in front of the driver during the convolution process. The most suitable window size is 160 feet in this case.

TABLE 2. Sensitivity analysis: Convolution window size on model performance.

Convolution Window	RSE of Model with Linear Kernel (%)	RSE of Model with Constant Kernel (%)
60	**13.71**	21.32
80	14.68	20.83
100	14.76	20.68
120	15.10	19.43
140	15.84	19.56
160	15.74	**19.41**
180	17.56	20.98
200	18.25	20.83

V. CONCLUSION

In conclusion, this work propels the field of macroscopic traffic flow modeling forward by addressing the boundedness issue inherent in previous models. A nonlocal LWR model paired with Greenshields fundamental diagram was chosen for analysis, and the well-posedness of the model and boundedness of the states were established within the previously established framework in the literature. The resolution of this limitation in the chosen model paves the way for more realistic and practical traffic modeling. The implementation of the Lax-Friedrichs algorithm, augmented with
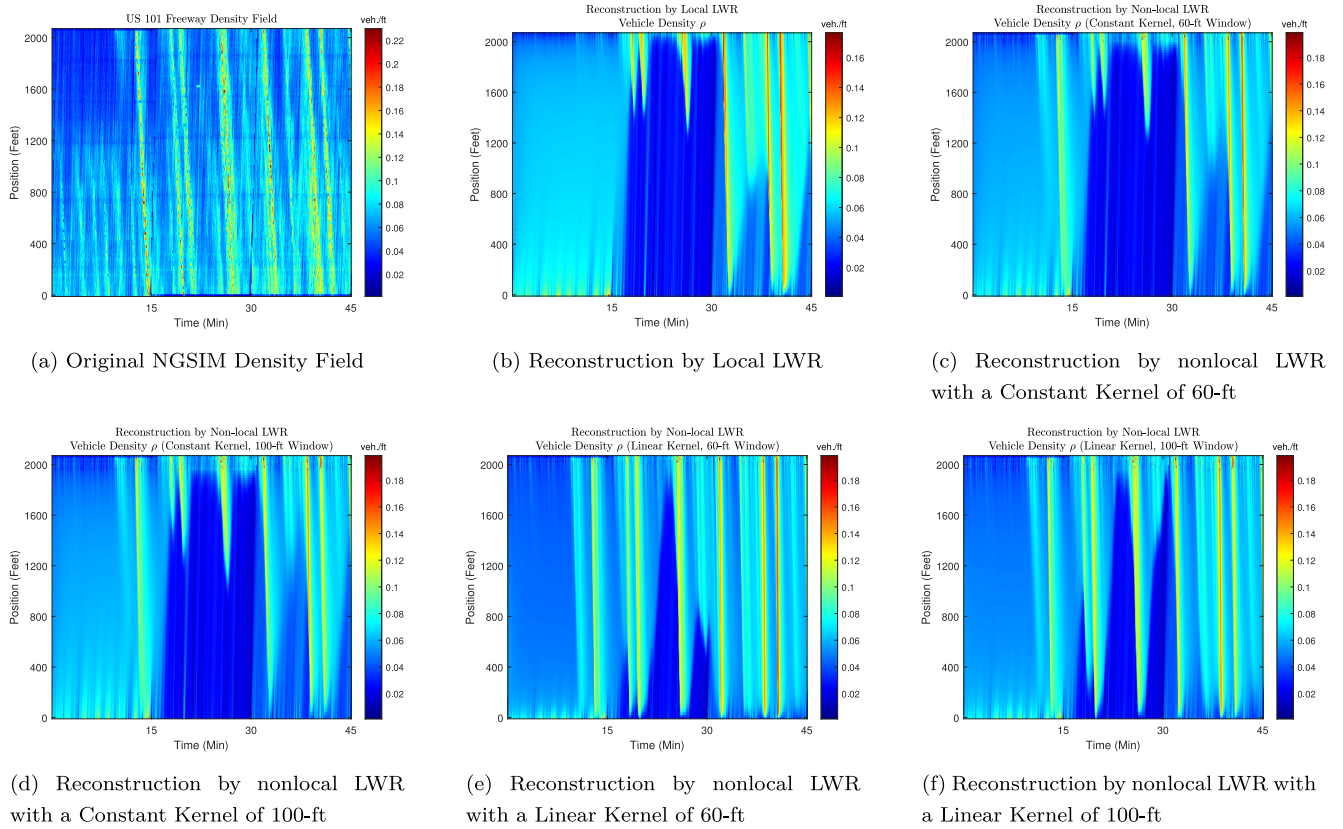
(a) Original NGSIM Density Field

(b) Reconstruction by Local LWR

(c) Reconstruction by nonlocal LWR with a Constant Kernel of 60-ft

(d) Reconstruction by nonlocal LWR with a Constant Kernel of 100-ft

(e) Reconstruction by nonlocal LWR with a Linear Kernel of 60-ft

(f) Reconstruction by nonlocal LWR with a Linear Kernel of 100-ft

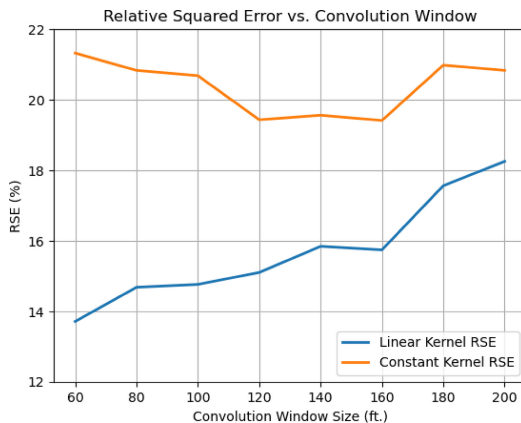**FIGURE 7.** The NGSIM Dataset and Reconstructions.

FIGURE 8. Convolution Window Size on Nonlocal Model Performance.

two look-ahead kernels, provides a scheme for numerically stable and accurate traffic field reconstruction. Through validation using the NGSIM dataset, we demonstrate that the proposed nonlocal model outperforms its local counterparts in capturing real-world traffic flow patterns. Furthermore, the design of two look-ahead kernels and the sensitivity analysis to identify the optimal look-ahead window size provide valuable insights. Thus, this research makes important theoretical and practical contributions to the field of traffic flow modeling. In future work, other fundamental diagrams such as the inverse-lambda shaped fundamental diagram [35], and triangular fundamental diagram [36] can be considered

in conjugation with nonlocal traffic flow models. The Well-posedness of these models, boundedness of the states, and field validation will be promising future research directions.

REFERENCES

[1] S. Blandin and P. Goatin, "Well-posedness of a conservation law with non-local flux arising in traffic flow modeling," *Numerische Mathematik*, vol. 132, no. 2, pp. 217–241, 2016.

[2] P. Goatin and S. Scialanga, "Well-posedness and finite volume approximations of the LWR traffic flow model with non-local velocity," *Netw. Heterogeneous Media*, vol. 11, no. 1, pp. 107–121, 2016.

[3] Q. Du, J. R. Kamm, R. B. Lehoucq, and M. L. Parks, "A new approach for a nonlocal, nonlinear conservation law," *SIAM J. Appl. Math.*, vol. 72, no. 1, pp. 464–487, 2012.

[4] E. Abreu, R. De la Cruz, J. Juajibioy, and W. Lambert, "Lagrangian-Eulerian approach for nonlocal conservation laws," *J. Dyn. Differ. Equ.*, pp. 1–47, Jul. 2022. [Online]. Available: https://doi.org/10.1007/s10884-022-10193-8

[5] M. Treiber, A. Hennecke, and D. Helbing, "Derivation, properties, and simulation of a gas-kinetic-based, nonlocal traffic model," *Phys. Rev. E, Stat. Phys. Plasmas Fluids Relat. Interdiscip. Top.*, vol. 59, no. 1, p. 239, 1999.

[6] F. A. Chiarello, "An overview of non-local traffic flow models," in *Mathematical Descriptions of Traffic Flow: Micro, Macro and Kinetic Models.* Cham, Switzerland: Springer, 2021, pp. 79–91.

[7] A. Bressan and W. Shen, "On traffic flow with nonlocal flux: A relaxation representation," *Arch. Ration. Mech. Anal.*, vol. 237, no. 3, pp. 1213–1236, 2020.

[8] A. J. Huang, A. Biswas, and S. Agarwal, "Incorporating nonlocal traffic flow model in physics-informed neural networks," 2023, *arXiv:2308.11818.*

[9] R. M. Colombo, M. Garavello, and M. Lécureux-Mercier, "A class of nonlocal models for pedestrian traffic," *Math. Models Methods Appl. Sci.*, vol. 22, no. 4, 2012, Art. no. 1150023.

[10] B. Piccoli and F. Rossi, "Transport equation with nonlocal velocity in Wasserstein spaces: Convergence of numerical schemes," *Acta Applicandae Mathematicae*, vol. 124, no. 1, pp. 73–105, 2013.

[11] P. Amorim, R. M. Colombo, and A. Teixeira, "On the numerical integration of scalar nonlocal conservation laws," *ESAIM Math. Model. Numer. Anal.*, vol. 49, no. 1, pp. 19–37, 2015.

[12] M. J. Lighthill and G. B. Whitham, "On kinematic waves. I: Flow movement in long rivers. II: A theory of traffic on long crowded roads," *Proc. Roy. Soc. London Series A*, vol. A229, no. 1178, pp. 281–345, 1955.

[13] G. B. Whitham, *Linear and Nonlinear Waves*. Hoboken, NJ, USA: Wiley, 2011.

[14] P. I. Richards, "Shockwaves on the highway," *Operat. Res.*, vol. 4, pp. 42–51, Feb. 1956.

[15] B. D. Greenshields, "A study in highway capacity," in *Proc. Highway Res. Board*, 1935 pp. 448–477.

[16] H. Greenberg, "An analysis of traffic flow," *Operat. Res.*, vol. 7, no. 1, pp. 78–85, 1959.

[17] R. T. Underwood, *Speed, Volume, and Density Relationships: Quality and Theory of Traffic Flow*. New Haven, CT, USA: Yale Bureau Highway Traffic, 1961, pp. 141–188.

[18] J. Drake, J. Schofer, and A. May, "A statistical analysis of speed-density hypotheses," in *Proc. 3rd Int. Symp. Theory Traffic Flow*, 1967, pp. 53–87.

[19] A. Schadschneider, "Statistical physics of traffic flow," *Physica A Stat. Mechan. Appl.*, vol. 285, nos. 1–2, pp. 101–120, 2000.

[20] B. S. Kerner, "The physics of traffic," *Phys. World*, vol. 12, no. 8, p. 25, 1999.

[21] M. Garavello and B. Piccoli, *Traffic Flow on Networks*, vol. 1. Springfield, MO, USA: Amer. Inst. Math. Sci., 2006.

[22] C. De Filippis and P. Goatin, "The initial–boundary value problem for general non-local scalar conservation laws in one space dimension," *Nonlinear Anal.*, vol. 161, pp. 131–156, Sep. 2017.

[23] F. Otto, "Initial-boundary value problem for a scalar conservation law," *Comptes rendus de l'Académie des sciences. Série 1, Mathématique*, vol. 322, no. 8, pp. 729–734, 1996.

[24] C. Bardos, A.-Y. LeRoux, and J.-C. Nédélec, "First order quasilinear equations with boundary conditions," *Commun. Partial Differ. Equ.*, vol. 4, no. 9, pp. 1017–1034, 1979.

[25] F. Dubois and P. Le Floch, "Boundary conditions for nonlinear hyperbolic systems of conservation laws," *J. Differ. Equ.*, vol. 71, no. 1, pp. 93–122, 1988.

[26] K. H. Karlsen, K.-A. Lie, and N. H. Risebro, "A front tracking method for conservation laws with boundary conditions," in *Hyperbolic Problems: Theory, Numerics, Applications*. Basel, Switzerland: Birkhäuser, 1999, pp. 493–502.

[27] R. Courant, K. Friedrichs, and H. Lewy, "Über die partiellen differenzengleichungen der mathematischen Physik," *Mathematische Annalen*, vol. 100, no. 1, pp. 32–74, 1928.

[28] (U.S. Dept. Transp., Washington, DC, USA). "FHWA, 2008a. NGSIM–next generation simulation." Accessed: May 24, 2021. [Online]. Available: https://datahub.transportation.gov/stories/s/i5zb-xe34

[29] A. M. Avila, *Applications of Koopman Operator Theory to Highway Traffic Dynamics*. Santa Barbara, CA, USA: Univ. California, 2017.

[30] D. Ni, *Traffic Flow Theory: Characteristics, Experimental Methods, and Numerical Techniques*. Oxford, U.K.: Butterworth-Heinemann, 2015.

[31] A. J. Huang and S. Agarwal, "Physics informed deep learning for traffic state estimation," in *Proc. IEEE 23rd Int. Conf. Intell. Transp. Syst. (ITSC)*, 2020, pp. 1–6.

[32] A. M. Avila and I. Mezić, "Data-driven analysis and forecasting of highway traffic dynamics," *Nat. Commun.*, vol. 11, no. 1, pp. 1–16, 2020.

[33] A. J. Huang and S. Agarwal, "Physics-informed deep learning for traffic state estimation: Illustrations with LWR and CTM models," *IEEE Open J. Intell. Transp. Syst.*, vol. 3, pp. 503–518, 2022.

[34] A. J. Huang and S. Agarwal, "On the limitations of physics-informed deep learning: Illustrations using first-order hyperbolic conservation law-based traffic flow models," *IEEE Open J. Intell. Transp. Syst.*, vol. 4, pp. 279–293, 2023.

[35] M. Koshi, "Some findings and an overview on vehicular flow characteristics," in *Proc. 8th Int. Symp. Transp. Traffic Theory*, 1983, pp. 403–451.

[36] C. Daganzo, *Fundamentals of Transportation and Traffic Operations*, vol. 30. Oxford, U.K.: Pergamon, 1997.

PUSHKIN KACHROO (Senior Member, IEEE) received the first Ph.D. degree in mechanical engineering from the University of California at Berkeley performing research in vehicle control, the second Ph.D. degree in mathematics from Virginia Tech in the area of hyperbolic system of partial differential equations with applications to traffic control and evacuation, and the third Ph.D. degree in physics from the University of Nevada Las Vegas, on the topic of Quantum Logic and Computation, where he is the Lincy chaired Professor with the Department of Electrical and Computer Engineering. He has been a Professor with Virginia Tech and a Visiting Professor with University of California at Berkeley. He has also been a Visiting Professor with IIT Delhi, IIT Bombay, and IIT Jammu. His M.S. degrees are from Rice University, Virginia Tech, and UNLV, and his B.Tech. from IIT Bombay in Civil Engineering. He is finishing another M.S. degree from IIT Delhi in Traffic Safety. He has published more than 200 journal and conference papers, including eleven books and four collected volumes.

SHAURYA AGARWAL (Senior Member, IEEE) received the B.Tech. degree in electronics and communication engineering from the Indian Institute of Technology Guwahati, Guwahati, and the Ph.D. degree in electrical engineering from the University of Nevada, Las Vegas, in 2015. He is currently an Assistant Professor with the Civil, Environmental, and Construction Engineering Department, University of Central Florida. He is the founding Director of the Urban Intelligence and Smart City (URBANITY) Lab. He was previously an Assistant Professor with the Electrical and Computer Engineering Department, California State University, Los Angeles, from 2016 to 2018. He was a Postdoctoral Research Fellow with New York University in 2016. As of March 2023, he has published a book, over 30 peer-reviewed journal publications, and multiple conference papers. His research focuses on interdisciplinary areas of cyber–physical systems, smart and connected transportation, and connected and autonomous vehicles. Passionate about cross-disciplinary research, he integrates control theory, information science, data-driven techniques, and mathematical modeling in his work. His work has been funded by several private and government agencies. He serves as an *Associate Editor* for IEEE TRANSACTIONS ON INTELLIGENT TRANSPORTATION SYSTEMS.

ANIMESH BISWAS received the bachelor's degree in electronics and telecommunication engineering from Jadavpur University, India, in 2007, the first master's degree from Indian Institute of Technology Madras, Chennai, in 2009, the second master's degree in electrical engineering from Iowa State University in 2015, and the Ph.D. degree in mathematics from Iowa State University in 2020. He is currently a Postdoctoral Faculty Fellow with the Mathematics Department, University of Nebraska–Lincoln. His research areas include the analysis of partial differential equations, specifically in the field of nonlocal modeling. He is a member of American Mathematical Society.
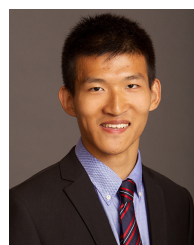
ARCHIE J. HUANG (Member, IEEE) received the B.Eng. degree in electrical engineering from Tsinghua University, the M.S. degree in applied urban science and informatics from New York University, and the Ph.D. degree in civil engineering from the University of Central Florida. He was a Senior Researcher with the Electrical and Computer Engineering Department, California State University, Los Angeles. His research and work interests include the fleet rebalancing problem of shared mobility services, simulation with connected and autonomous vehicles, traffic modeling with variable speed limits, and physics-informed deep learning for traffic state estimation.